SCIENCE AND TECHNOLOGY ORGANIZATION
CENTRE FOR MARITIME RESEARCH AND EXPERIMENTATION

Reprint Series **CMRE-PR-2017-001**

Separation of measured noise coherence matrix into Toeplitz and Hankel parts

Chris H. Harrison

August 2017

Originally published in:

Journal of the Acoustical Society of America, Vol. 141, No.4, April 2017, pp. 2812–2820.

About CMRE

The Centre for Maritime Research and Experimentation (CMRE) is a world-class NATO scientific research and experimentation facility located in La Spezia, Italy.

The CMRE was established by the North Atlantic Council on 1 July 2012 as part of the NATO Science & Technology Organization. The CMRE and its predecessors have served NATO for over 50 years as the SACLANT Anti-Submarine Warfare Centre, SACLANT Undersea Research Centre, NATO Undersea Research Centre (NURC) and now as part of the Science & Technology Organization.

CMRE conducts state-of-the-art scientific research and experimentation ranging from concept development to prototype demonstration in an operational environment and has produced leaders in ocean science, modelling and simulation, acoustics and other disciplines, as well as producing critical results and understanding that have been built into the operational concepts of NATO and the nations.

CMRE conducts hands-on scientific and engineering research for the direct benefit of its NATO Customers. It operates two research vessels that enable science and technology solutions to be explored and exploited at sea. The largest of these vessels, the NRV Alliance, is a global class vessel that is acoustically extremely quiet.

CMRE is a leading example of enabling nations to work more effectively and efficiently together by prioritizing national needs, focusing on research and technology challenges, both in and out of the maritime environment, through the collective Power of its world-class scientists, engineers, and specialized laboratories in collaboration with the many partners in and out of the scientific domain.

NOTE: The CMRE Reprint series reprints papers and articles published by CMRE authors in the open literature as an effort to widely disseminate CMRE products. Users are encouraged to cite the original article where possible.

Separation of measured noise coherence matrix into Toeplitz and Hankel parts

Chris H. Harrison[a)]
Emeritus Scientist, Centre for Maritime Research and Experimentation, Viale San Bartolomeo 400, 19126 La Spezia, Italy

(Received 30 November 2016; revised 3 April 2017; accepted 4 April 2017; published online 20 April 2017)

The cross-spectral density of ocean ambient noise is usually estimated from the product of the complex hydrophone signals, each of which already corresponds to the summed responses of sources from all angles. The true coherence is the integral over all angles of the angle-dependent product. The influence of this distinction on necessary time integration in geoacoustic inversion and passive fathometry is explored, and a meaningful separation of the cross-spectral density matrix into Toeplitz and Hankel parts is proposed. Various processing techniques are applied to synthesized data and some experimental vertical array data in a passive fathometry context. Passive fathometry is only sensitive to the Hankel part of the matrix. © *2017 Acoustical Society of America*.
[http://dx.doi.org/10.1121/1.4981120]

[SED] Pages: 2812–2820

I. INTRODUCTION

In recent years ocean ambient noise has been used as a sound source of opportunity to measure such environmental properties as seabed reflection coefficient (Harrison and Simons, 2002; Quijano *et al.*, 2012; Muzi *et al.*, 2015), and sub-bottom profiles by either restoring the reflection phase through spectral factorization (Harrison, 2004, 2005), or "passive fathometry" (Siderius *et al.*, 2006; Harrison and Siderius, 2008; Gerstoft *et al.*, 2008; Siderius *et al.*, 2010; Traer and Gerstoft, 2011). The signal processing in all these cases is based, one way or another, on the noise coherence or cross-spectral-density-matrix (CSDM) measured by an acoustic array. If adaptive beam forming (ABF) rather than conventional (CBF) is to be used then the CSDM must be invertible, but above all, regardless of the method or the aim, some time averaging is required. The usual method of achieving this averaging is to Fourier transform blocks of multiple hydrophone data from time to acoustic frequency. At a single frequency the CSDM, $\mathbf{C}$, with components $C_{n,m}$, is formed from the vector of N hydrophone inputs with individual elements x_n by running a continuous loop to construct a time average,

$$C_{n,m} = C_{n,m} + x_n x_m^*; \quad 1 \le n, m \le N\,. \tag{1}$$

Throughout this paper scalars (with possible subscripts) are denoted as italics, and their conjugates are indicated by an asterisk. Matrices and vectors will be shown in bold with conjugate transpose indicated by a dagger. The desired average of spatial coherence is the sum over all angles of *the product of* $x_n\, x_m^*$; however, each element of $\mathbf{x}$ is, independently, already a sum (or integral) of noise sources over all angles. This is one of three possible reasons for needing to time-average in the case of passive fathometry. In total these reasons are as follows:

(1) To achieve convergence of the up- and down-beam cross-correlation to form the impulse response of the virtual source in passive fathometry.
(2) To build a full-rank CSDM in order to invert it (in the case of ABF processing).
(3) To achieve convergence of $x_n\, x_m^*$ to $\langle x_n\, x_m^* \rangle$ by eliminating angular cross-terms as mentioned above.

A search for an alternative way of tackling the unwanted angular cross-terms of the third reason above has led from the standard method ("method 1," below) first to a formulation in which the CSDM is derived in terms of an explicit Toeplitz component and an explicit Hankel component ("method 2"), then to a simplified but familiar approach ("method 3") that avoids use of matrices altogether. Both latter methods appear to bypass the usual need for explicit time-averaging (although it transpires that this impression is illusory), and the third method is extremely fast computationally.

The reason for interest in the processing details is that a vertical component of motion of the hydrophone array minimises the time available for integration. This motion may be unintentional, for example caused by wave motion of a vertical array in bad weather (Harrison and Siderius, 2008; see also Sec. III below) or intentional when a small array is attached to a glider that is constantly, but slowly changing depth. The remainder of this paper compares these three methods.

II. THREE PROCESSING APPROACHES

A. Method 1: The standard approach

Initially we postulate generalised, distant sources at elevation angle θ with complex amplitude $a(\theta)$, implicitly a function of frequency. Experimentally what is received at the hydrophone depth z_n is the integral of the arrivals over all angles

[a)]Also at Institute of Sound and Vibration Research, University of Southampton, Highfield, Southampton SO17 1BJ, United Kingdom. Electronic mail: chris.harrison1946@gmail.com

$$x_n = \int_{-\pi/2}^{\pi/2} a(\theta) \exp(ikz_n \sin\theta) \cos\theta \, d\theta. \quad (2)$$

The CSDM is constructed from an average of the form given in Eq. (1). Substituting Eq. (2) into Eq. (1) makes the result clear

$$C_{n,m} = \int_{-\pi/2}^{\pi/2} \int_{-\pi/2}^{\pi/2} a(\theta_1)\, a^*(\theta_2) \exp(ikz_n \sin\theta_1) \times \exp(-ikz_m \sin\theta_2) \cos\theta_1 \cos\theta_2 \; d\theta_1 d\theta_2, \quad (3)$$

which can be written in terms of $X_{1,2} \equiv \sin\theta_{1,2}$ as

$$C_{n,m} = \int_{-1}^{1} \int_{-1}^{1} a(X_1)\, a^*(X_2) \exp(ikz_n X_1) \times \exp(-ikz_m X_2) dX_1 dX_2. \quad (4)$$

After substantial time averaging, all the cross terms ($\theta_2 \neq \theta_1$ or $\theta_2 \neq -\theta_1$) sum to zero, so what remains is (in underwater acoustics, provided the sources are either distant or nearly overhead, $\theta_2 = \pm\theta_1$) $X_2 = X_1$ and $X_2 = -X_1$,

$$\begin{aligned} C_{n,m} = & \int_0^1 a(+X_1)a^*(+X_1) \exp\left(+ik(z_n - z_m)X_1\right) dX_1 \\ & + \int_0^1 a(-X_1)a^*(-X_1) \exp\left(-ik(z_n - z_m)X_1\right) dX_1 \\ & + \int_0^1 a(+X_1)a^*(-X_1) \exp\left(ik(z_n + z_m)X_1\right) dX_1 \\ & + \int_0^1 a(-X_1)a^*(+X_1) \exp\left(-ik(z_n + z_m)X_1\right) dX_1. \end{aligned} \quad (5)$$

This can be seen to be a simplified version (vertical separation, loss-free) of the formula for noise coherence given by Harrison (1996) with a multiplier of $\sin\theta/(1 - RR^*)$ absorbed in the source amplitudes a, and $a(+X) = 1$, $a(-X) = R \exp(i2kh)$ with R being (complex) seabed reflection coefficient and h being water depth. So the correspondence is

$$\begin{aligned} a(+X)a^*(+X) &= 1, \\ a(-X)a^*(-X) &= RR^*, \\ a(+X)a^*(-X) &= R^* \exp(-i2kh), \\ a(-X)a^*(+X) &= R \exp(i2kh). \end{aligned}$$

Note that, if the sources are not distant or overhead, then for any amount of refraction, arbitrary hydrophone displacement, or proximity to boundaries there will always be a θ_1, θ_2 pair at the respective hydrophones that define corresponding rays (possibly including reflections) that project backward to meet at a common source (possibly with finite size), whereas all others lead to uncorrelated parts of the sea surface. So out of all the θ_1, θ_2 pairs, only one pair links the source to the two hydrophones. Although this coincidence may not be at exactly $\theta_2 = \theta_1$ or $\theta_2 = -\theta_1$ it will be close enough that the effects of array size and refraction on the following analysis are very small.

Thus method 1, the standard approach, consists of forming a time average of $\mathbf{C}$, and then, according to one's ultimate aims, (e.g., passive fathometry, reflection loss vs angle, ABF vs CBF), forming terms such as, $\mathbf{v}^\dagger\mathbf{C}\mathbf{w}$, $\mathbf{v}^\dagger\mathbf{C}\mathbf{v}$, $\mathbf{v}^\dagger\mathbf{C}^{-1}\mathbf{w}$, given steering vectors $\mathbf{v}$, $\mathbf{w}$. These matrix operations lead to estimates of reflection loss, seabed impulse response, and so on (e.g., see Harrison and Simons, 2002; Harrison and Siderius, 2008; Harrison, 2009).

B. Method 2: Separation of the Toeplitz and Hankel parts

From Eq. (5), whatever $a()$ is, the time-averaged $\mathbf{C}$ naturally separates into Toeplitz and Hankel parts, provided the hydrophones are uniformly spaced, since the first two lines depend on $(n - m)$ and the third and fourth lines depend on $(n + m)$, i.e., $\mathbf{C} \equiv \mathbf{T} + \mathbf{H}$. It is convenient to separate the upper part of the field from the lower part by introducing the notation

$$\begin{aligned} U(X) &= a(+X), \\ D(X) &= a(-X), \end{aligned} \quad 0 < X < 1\,, \quad (6)$$

with $X \equiv \sin\theta$, having dropped the subscript of X:

$$\begin{aligned} T_{n,m} &= \int_{-1}^{1} a(+X)a^*(+X) \exp\left(+ik(z_n - z_m)X\right) dX \\ &= \int_0^1 U(X)U^*(X) \exp\left(ik(z_n - z_m)X\right) dX \\ &\quad + \int_0^1 D(X)D^*(X) \exp\left(-ik(z_n - z_m)X\right) dX, \end{aligned} \quad (7)$$

$$\begin{aligned} H_{n,m} &= \int_{-1}^{1} a(+X)a^*(-X) \exp\left(ik(z_n + z_m)X\right) dX \\ &= \int_{-1}^{1} a(-X)a^*(+X) \exp\left(-ik(z_n + z_m)X\right) dX \\ &= \int_0^1 U(X)D^*(X) \exp\left(ik(z_n + z_m)X\right) dX \\ &\quad + \int_0^1 D(X)U^*(X) \exp\left(-ik(z_n + z_m)X\right) dX \\ &= 2 \times \text{real} \left[\int_0^1 U(X)D^*(X) \exp\left(ik(z_n + z_m)X\right) dX \right]. \end{aligned} \quad (8)$$

Note that, by symmetry, all Hankel elements are real.

Returning to the original observation that without considerable averaging $x_n\, x_m^*$ is not, after all, the desired coherence it can be seen that these ready-averaged integrals are, in fact, spatial auto- or cross-correlations of x_n expressed in terms of Fourier transforms into the angle domain. This suggests that one can construct them directly from the given x_n without any further time-averaging to eliminate angular cross-terms (third type listed in Sec. I).

To construct the Toeplitz part one first takes the inverse Fourier transform (IFT) of x_n to *estimate* effective sources at infinity (strength $\hat{a}$)

$$\hat{a}(\theta) = \sum_{n=1}^{N} x_n \exp(-ikz_n \sin\theta), \tag{9}$$

where $\hat{a}(\theta)$ is some kind of (instantaneous) effective noise source that results in the known signals x_n at the hydrophones. Then one takes the modulus square of this quantity and Fourier transforms it back to a hydrophone separation Z^T $(\equiv z_n - z_m)$,

$$T^E(Z^T) = \int_{-\pi/2}^{\pi/2} |\hat{a}(\theta)|^2 \exp(ikZ^T \sin\theta) \cos\theta \, d\theta. \tag{10}$$

This T^E is already the same as the desired T, as in Eq. (7), except for the hat, meaning "estimate." Thinking of $|\hat{a}(\theta)|^2$ as a "power spectrum," the integral in Eq. (10), being its Fourier transform, is the auto-correlation function of the hydrophone signal x, at this acoustic frequency. This relation can be made exact by assuming equal hydrophone spacing $Z^T \equiv (n-m)d$, and discretizing $\sin\theta$ between -1 and $+1$ at intervals of

$$\Delta = \frac{2\pi}{Nkd}, \tag{11}$$

so $\sin\theta \equiv j\Delta$, then turning the Fourier series relationship between Eqs. (9) and (10) into a discrete Fourier transform[1] (DFT):

$$T^E{}_\nu = \sum_{j=1}^{N} |a_j|^2 \exp(i2\pi j\nu/N). \tag{12}$$

The single subscript of $T^E{}_\nu$ signifies the offset from the main diagonal. Thus, inserting Eq. (9) into Eq. (10) yields $T^E{}_\nu$ as an autocorrelation function of x_n,

$$T^E{}_\nu = \sum x_n{}^* x_{\nu+n}, \tag{13}$$

where for each offset, ν, as $x_{\nu+n}$ slides over x_n the sum is taken over the overlapping portion only, and

$$\begin{aligned} z_n &= n\,d, \\ Z^T{}_\nu &= \nu d. \end{aligned} \tag{14}$$

This sum, as defined above, is identical to a sum down the νth diagonal of the matrix $\mathbf{x}\mathbf{x}^\dagger$. In other words the Toeplitz matrix is simply formed by summing along the appropriate diagonals of the given coherence matrix.[2] The first benefit of this approach is that this simple Fourier transforming operation appears to have bypassed the need for time-averaging to eliminate angular cross-terms (third type listed in Sec. I) to arrive directly at the angle integral of the true coherence function, as in Eq. (12) [or Eq. (10)]. The second benefit is that for any beam-forming application the symmetry of this, guaranteed, Toeplitz matrix enables possible extensions to the effective array size (Muzi *et al.*, 2015) and possible "filling" out of nested arrays (where hydrophone spacings, though multiples of a single value, are irregular) (Young, 2005). Equations (10) and (9) show explicitly that it is possible to separate out the Toeplitz part of any experimental data from a uniformly spaced vertical array.

The Hankel part, Eq. (8), can be constructed in a similar way. The sources $\hat{a}(\theta)$ are estimated as in Eq. (9) but instead of modulus-squaring them, $\hat{a}(\theta)$ is multiplied by its up-down-reverse $\hat{a}(-\theta)$ then the product is Fourier transformed back to a hydrophone separation Z^H $(\equiv z_n + z_m)$,

$$H^E(Z^H) = \int_{-\pi/2}^{\pi/2} \hat{a}(\theta)\hat{a}(-\theta)^* \exp(+ikZ^H \sin\theta) \cos\theta \, d\theta. \tag{15}$$

This integral is the frequency domain representation of the cross-correlation function of the signal vector x_n with its reverse x_{N-n} at this acoustic frequency. It also corresponds to the Fourier transform of the convolution of x with itself. Again these relations are made exact by discretizing $\sin\theta$ as in Eq. (11). Thus, inserting Eq. (9) into Eq. (15) yields the convolution

$$H^E{}_\nu = \sum x_n x_{(\nu+N)-n}, \tag{16}$$

where for each offset, ν, as $x_{(\nu+N)-n}$ slides over x_n the sum is again taken over the overlapping portion only, and

$$\begin{aligned} z_n &= n\,d, \\ Z^H{}_\nu &= \nu d. \end{aligned} \tag{17}$$

So the Hankel matrix may be constructed simply by summing along the appropriate anti-diagonals of the given coherence matrix $\mathbf{x}\mathbf{x}^\dagger$.

Passive fathometry is independent of the Toeplitz part and only depends on the Hankel part (Harrison, 2009). It is therefore useful to be able to separate it out.

So now "method 2" consists of using Eqs. (9), (10), and (15) to calculate a Toeplitz matrix $\mathbf{T}$ and a Hankel matrix $\mathbf{H}$. The combined coherence $\mathbf{C}$,

$$\mathbf{C} = \mathbf{T} + \mathbf{H} \tag{18}$$

is used to calculate terms such as, $\mathbf{v}^\dagger\mathbf{C}\mathbf{w}$, $\mathbf{v}^\dagger\mathbf{C}\mathbf{v}$, $\mathbf{v}^\dagger\mathbf{C}^{-1}\mathbf{w}$, as before. ABF processing, if needed, may still require the time-averaging to achieve full rank (second type listed in Sec. I), and passive fathometry still requires time-averaging to extract the impulse response from the cross-correlation (first type in the list).

C. Method 3: Connection to a simple solution

The respective symmetries of the Toeplitz and Hankel arrays allow the one-dimensional representations as in Eqs. (10) and (15) but these are obviously simply related to the usual two-dimensional representation, Eq. (5). Inspection of this result and subsequent matrix multiplication by the up-, down-steering vectors will show that the whole operation can be simplified and checked against alternative well known formulations.

Generally, whether forming a beam or sub-bottom profiling with noise, the matrix operations involve forming a

product $\mathbf{w}^\dagger\mathbf{C}\mathbf{v}$ with two different steering vectors $\mathbf{w}$, $\mathbf{v}$. This operation is identical to an element-by-element summation over all elements of $\mathbf{C}$ multiplied by the matrix $\mathbf{W}$ formed of the steering vectors alone, $\mathbf{W} = \mathbf{w}\mathbf{v}^\dagger$, where

$$w_n(\theta_1) = \exp(ikz_n \sin\theta_1),$$
$$v_n(\theta_2) = \exp(ikz_n \sin\theta_2),$$

i.e.,

$$\mathbf{w}^\dagger\mathbf{C}\mathbf{v} = \sum_n^N \sum_m^N C_{n,m} W_{n,m}. \tag{19}$$

If $\mathbf{v} = \mathbf{w}$, i.e., $\theta_2 = \theta_1$, as is true when forming a beam, then $\mathbf{W}$ is Toeplitz; if $\mathbf{v} = \mathbf{w}^\dagger$, i.e., $\theta_2 = -\theta_1$, or in particular, $|\theta_2| = |\theta_1| = \pi/2$, as is true with sub-bottom profiling or passive fathometry, then $\mathbf{W}$ is Hankel.

Therefore when forming a beam the diagonal symmetry of $\mathbf{W}$ matches that of $\mathbf{T}$ but not the anti-diagonal symmetry of $\mathbf{H}$. In contrast, with passive fathometry, the anti-diagonal symmetry of $\mathbf{W}$ matches that of $\mathbf{H}$ but not the diagonal symmetry of $\mathbf{T}$. The product of this mismatch tends to zero. This incidentally demonstrates that passive fathometry is completely independent of $\mathbf{T}$.

So to be specific in forming vertical beams, denoting a vertically "up" steering vector as $\mathbf{w_U}$ and down as $\mathbf{w_D}$, one obtains

$$\mathbf{w_U}^\dagger\mathbf{C}\mathbf{w_U} \cong \sum_n^N \sum_m^N T_{n,m} W^{UU}{}_{n,m}, \tag{20}$$

$$\mathbf{w_D}^\dagger\mathbf{C}\mathbf{w_D} \cong \sum_n^N \sum_m^N T_{n,m} W^{DD}{}_{n,m}, \tag{21}$$

where

$$W^{UU}{}_{n,m} = \exp\left(-ik(z_n - z_m)\right), \tag{22}$$

$$W^{DD}{}_{n,m} = \exp\left(ik(z_n - z_m)\right), \tag{23}$$

but because of the symmetry, the double sum of Eqs. (20) and (21) can be written as a single sum along the anti-diagonals with a weight determined by the sum along the diagonal. Thus,

$$\sum_n^N \sum_m^N T_{n,m} W^{UU}{}_{n,m} = \sum_{j=-(N-1)}^{N-1} (N - |j|)\, T_{j+N} \exp(-ikZ^T{}_{j+N}), \tag{24}$$

where the single index j counts from the bottom-left to the top-right of the matrix $\mathbf{T}$, and $j = 0$ corresponds to the diagonal of $\mathbf{T}$, i.e., $n = m$, and $Z^T{}_j = z_n - z_m$.

In passing, it is worth noting that the single sums going from $j = -(N-1)$ to $+(N-1)$ in Eqs. (24) show that hidden in the matrix is useful information from a "virtual" hydrophone array with $1 + 2(N-1) = 2N-1$ elements, rather than the true N, but with non-uniform weightings of $(N - |j|)$. This is an explanation of the improved resolution found by Muzi *et al.* (2015).

The passive fathometer UD and DU terms may be determined in a similar fashion as

$$\mathbf{w_U}^\dagger\mathbf{C}\mathbf{w_D} \cong \sum_n^N \sum_m^N H_{n,m} W^{UD}{}_{n,m}, \tag{25}$$

$$\mathbf{w_D}^\dagger\mathbf{C}\mathbf{w_U} \cong \sum_n^N \sum_m^N H_{n,m} W^{DU}{}_{n,m}, \tag{26}$$

where

$$W^{UD}{}_{n,m} = \exp\left(-ik(z_n + z_m)\right), \tag{27}$$

$$W^{DU}{}_{n,m} = \exp\left(ik(z_n + z_m)\right), \tag{28}$$

but because of the symmetry, the double sum can again be written as a single sum in the diagonal direction with a weight determined by the sum in the anti-diagonal direction.

Thus,

$$\sum_n^N \sum_m^N H_{n,m} W^{UD}{}_{n,m} = \sum_{j=-(N-1)}^{N-1} (N - |j|)\, H_{j+N} \exp(-ikZ^H{}_{j+N}), \tag{29}$$

where $j = 0$ corresponds to the anti-diagonal of $\mathbf{H}$, i.e., $n = -m$, and $Z^H{}_j = z_n + z_m$.

In both cases the single sums [respectively Eqs. (24) for $\mathbf{T}$ and (29) for $\mathbf{H}$] resemble a Fourier transform. But already $\mathbf{T}$ consists of the product of a function of angle with its conjugate, Fourier transformed back to hydrophone position-space. Similarly $\mathbf{H}$ consists of the product of a function of up-angle with a corresponding function of down-angle, Fourier transformed back to hydrophone position-space. Thus they are both a backward transform of a forward transform (ignoring the weighting for the time being). This suggests that instead of performing this double transform we could have simply selected the "up" and the "down" *value* from the already existing functions of angle.

1. Toeplitz part

An exact result is found first for the Toeplitz part by substituting Eq. (10) into Eq. (24). Thus,

$$\mathbf{w_U}^\dagger\mathbf{T}\mathbf{w_U} = \sum_{j=-(N-1)}^{N-1} (N - |j|) \left(\int_{-1}^{1} |\hat{a}(X)|^2 \exp(ikZ^T{}_{j+N} X)\, dX \right) \times \exp(-ikZ^T{}_{j+N}). \tag{30}$$

Rearranging,

$$\mathbf{w_U}^\dagger\mathbf{T}\mathbf{w_U} = \int_{-1}^{1} |\hat{a}(X)|^2 \times \left[\sum_{j=-(N-1)}^{N-1} (N - |j|) \exp(ikZ^T{}_{j+N}(X-1)) \right] dX. \tag{31}$$

The term in square brackets can now be seen as a simple double sum which can itself be written as a product, and the resulting exponential sum in the second line can be evaluated:

$$\begin{aligned}
&\mathbf{w_U}^\dagger \mathbf{T} \mathbf{w_U} \\
&= \int_{-1}^{1} |\hat{a}(X)|^2 \left[\sum_{n=1}^{N} \sum_{m=1}^{N} \exp\Big(ik(z_n - z_m)(X-1) \Big) \right] dX \\
&= \int_{-1}^{1} |\hat{a}(X)|^2 \left| \sum_{n=0}^{N-1} \exp(inkd\,(X-1)) \right|^2 dX \\
&= \int_{-1}^{1} |\hat{a}(X)|^2 \left(\frac{\sin\left(\frac{1}{2} Nkd(X-1)\right)}{\sin\left(\frac{1}{2} kd(X-1)\right)} \right)^2 dX. \qquad (32)
\end{aligned}$$

Taking the discretized $\sin\theta$ ($=X$), as in Eq. (11), the $\sin NY/\sin Y$ term in the last line becomes a delta function, and so

$$\mathbf{w_U}^\dagger \mathbf{T} \mathbf{w_U} = |\hat{a}(1)|^2 = \left| \sum_{n}^{N} x_n \exp(-ikz_n) \right|^2, \qquad (33)$$

where $\hat{a}(1)$ is given in terms of hydrophone inputs x_n by Eq. (9) with $\theta = \pi/2$. But for any matrix $\mathbf{R}$ defined by $\mathbf{R} = \mathbf{x}\,\mathbf{x}^\dagger$ the well-known identity

$$\mathbf{w_U}^\dagger \mathbf{R} \mathbf{w_U} = \mathbf{w_U}^\dagger \mathbf{x}\,(\mathbf{w_U}^\dagger \mathbf{x})^\dagger = |\mathbf{w_U}^\dagger \mathbf{x}|^2 \qquad (34)$$

demonstrates that this derivation has gone full circle in tying the Toeplitz and Hankel formulas of Eqs. (10), (13), (15), and (16) to the usual formulation of Eqs. (1) and (5). Thus, Eqs. (33) and (34) show that there is an exact separated $\mathbf{T}$ in the sense that $\mathbf{w_U}^\dagger \mathbf{T} \mathbf{w_U} = \mathbf{w_U}^\dagger \mathbf{C} \mathbf{w_U}$, where $\mathbf{C} = \mathbf{x}\,\mathbf{x}^\dagger$.

By a similar argument it is straightforward to show that

$$\mathbf{w_D}^\dagger \mathbf{T} \mathbf{w_D} = |\hat{a}(-1)|^2 = \left| \sum_{n}^{N} x_n \exp(+ikz_n) \right|^2. \qquad (35)$$

2. Hankel part

The Hankel part which is most important for passive fathometry can be evaluated by inserting Eq. (15) in Eq. (29),

$$\begin{aligned}
&\mathbf{w_D}^\dagger \mathbf{H} \mathbf{w_U} \\
&= \sum_{j=-(N-1)}^{N-1} (N - |j|) \int_{-1}^{1} \hat{a}(X) \hat{a}(-X)^* \\
&\quad \times \exp(+ikZ^H{}_{j+N} X)\, dX \exp(-ikZ^H{}_{j+N}) \\
&= \int_{-1}^{1} \hat{a}(X) \hat{a}(-X)^* \\
&\quad \times \left[\sum_{j=-(N-1)}^{N-1} (N - |j|) \exp\left(ikZ^H{}_{j+N} (X-1) \right) \right] dX. \qquad (36)
\end{aligned}$$

Now, since $Z^H{}_{j+N} \equiv z_n + z_m$ it is important to note that $\mathbf{H}$, i.e., the $\hat{a}$ terms, contain all the phase offsets that correspond to the upward and downward path differences. In contrast, the steering vectors represented by the contents of the square brackets contain no such phase offsets. Again this term can be broken down into a product of two single sums, but the second one is not conjugated as before. If one adopts the convention that the offsets are measured from the centre of the hydrophone array then the same convolution result is obtained as before [in Eq. (32)]

$$\begin{aligned}
&\mathbf{w_D}^\dagger \mathbf{H} \mathbf{w_U} \\
&= \int_{-1}^{1} \hat{a}(X) \hat{a}(-X)^* \left[\sum_{n=1}^{N} \sum_{m=1}^{N} \exp(ik(z_n + z_m)(X-1)) \right] dX \\
&= \int_{-1}^{1} \hat{a}(X) \hat{a}(-X)^* \left[\sum_{n=1}^{N} \exp(ikz_n(X-1)) \right. \\
&\quad \left. \times \sum_{m=1}^{N} \exp(ikz_m(X-1)) \right] dX. \qquad (37)
\end{aligned}$$

But since the phases have been chosen to be zero at the array centre the argument of either exponential could have been taken as positive or negative without altering the value of the sums. Therefore, this can again be written as

$$\begin{aligned}
&\mathbf{w_D}^\dagger \mathbf{H} \mathbf{w_U} \\
&= \int_{-1}^{1} \hat{a}(X) \hat{a}(-X)^* \left[\left| \sum_{n=0}^{N-1} \exp(inkd(X-1)) \right|^2 \right] dX \\
&= \int_{-1}^{1} \hat{a}(X) \hat{a}(-X)^* \left(\frac{\sin\left(\frac{1}{2} Nkd(X-1)\right)}{\sin\left(\frac{1}{2} kd(X-1)\right)} \right)^2 dX. \qquad (38)
\end{aligned}$$

Discretizing $\sin\theta$, i.e., X, as with Eq. (33) leads to the conclusion that

$$\begin{aligned}
\mathbf{w_D}^\dagger \mathbf{H} \mathbf{w_U} &= \hat{a}(+1)\,\hat{a}(-1) \\
&= \sum_{n}^{N} x_n \exp(-ikz_n) \times \sum_{n}^{N} x_n \exp(+ikz_n). \qquad (39)
\end{aligned}$$

This proves that there is an exact separated $\mathbf{H}$ in the sense that $\mathbf{w_D}^\dagger \mathbf{H} \mathbf{w_U} = \mathbf{w_D}^\dagger \mathbf{C} \mathbf{w_U}$, where $\mathbf{C} = \mathbf{x}\,\mathbf{x}^\dagger$. This simple result, with $\hat{a}(1)$ and $\hat{a}(-1)$ given in terms of the hydrophone inputs x_n by Eq. (9) with $\theta = \pm\pi/2$, is the basis of method 3.

Equation (39) provides a quantity that can be Fourier transformed from acoustic frequency to impulse-response-time and therefore sub-bottom depth profile. What is rather surprising is that its right hand side avoids use of matrices altogether. It has therefore avoided both the second and third time-averaging requirement mentioned in Sec. I.

In retrospect Eqs. (9), (10), and (15) for the separated Toeplitz and Hankel parts were written in terms of arbitrary hydrophone separations along a vertical line, and it was only

necessary to invoke uniform separation for Eqs. (13) and (16) and subsequent expansions in terms of **T** and **H**, such as Eqs. (24) and (29). In other words, Eq. (9) is still valid for non-uniform hydrophone separation, and therefore so are Eqs. (10) and (15), meaning that there exists an effective Toeplitz and Hankel separation of **C** even with arbitrary hydrophone separation where the diagonals of **C** would be distinctly not parallel. Needless to say, Eqs. (33), (34), (35), and (39) remain valid since they do not depend on hydrophone separation, whereas Eqs. (13) and (16) clearly do, and so would no longer be valid.

III. SUMMARY OF RESULTS

The behaviour of the calculated Toeplitz and Hankel matrices as integration time is increased can be simulated at a single frequency by postulating noise at the hydrophone with a random real and imaginary part that is a function of angle, $\phi_n(\theta)$. To simulate the correlation between upward and downward angles the same random numbers are used for corresponding components above and below horizontal, but the bottom reflected components may be reduced by a reflection coefficient factor R and a phase $\exp(2iknH\sin\theta)$ that represents the path length to the seabed and back. With this basis one can compute the "true" coherence as $C_{n,m}^{TRUE} = \int \phi_n(\theta)\phi_m{}^*(\theta)\cos\theta\, d\theta$, the usual "experimental" product of hydrophone inputs $C_{n,m}^{EXPT} = x_n x_m{}^* = \int \phi_n(\theta)\cos\theta\, d\theta \times \int \phi_m{}^*(\theta)\cos\theta\, d\theta$, and the Toeplitz and Hankel components as in the text $C_{n,m}^{T+H} = T_{n,m} + H_{n,m}$ using Eqs. (13) and (16). Each of these can be averaged by adding in the result of a new sequence of $\phi_n(\theta)$.

The upper row of panels in Fig. 1 shows surface plots of the CSDMs at 1.5 kHz for "True," "Expt," and "T+H" for an average over just ten realisations, and the lower row is the same but for 100 realisations. In this example the seabed is deliberately (and unrealistically) close to the 128 element array, with a round-trip path of 36 m, so that, concentrating on the "True" panels, the Hankel contribution can be clearly seen as the strong anti-diagonal that crosses the main diagonal near element 100. This is because, for this path difference and a hydrophone separation of 0.18 m the anti-diagonal is defined by $n+m = 36/0.18 = 200$, giving an intersection and a peak at $n = m = 100$. If the seabed had been further from the array the Hankel features, though still existent, would have been harder to discriminate by eye because the anti-diagonal ridge would have been beyond the bottom-right of the matrix.

In all three cases averaging has two effects: one is to even out fluctuations along the tops of the ridges; another is to reduce the "clutter" away from the ridges. As one might expect, the "true" CSDM is nearest to ideal because it is effectively ready-averaged (in the sense that there are already no angular cross terms), and therefore there is minimal difference between upper and lower panel. In contrast, the Expt CSDM is rather chaotic even after substantial averaging, although one can still detect the jagged ridges of the main diagonal and the anti-diagonal. The point of this figure is to compare the third column (T+H) with the second column (Expt). Even with a small amount of averaging T+H comes close to the ideal "True" case. Furthermore, even after substantial averaging T+H is much better than Expt in two respects: the floor values are smoother, and both diagonal and anti-diagonal ridges are smoother.

Despite the differences between the three CSDMs demonstrated in Fig. 1 the scalar products of the CSDMs with various combinations of up- and down-steering vectors that were described in Sec. II C obey certain equalities or near-equalities, namely,

- For both steering vectors in the same direction

$$\mathbf{w_U}^\dagger \mathbf{T} \mathbf{w_U} = \mathbf{w_U}^\dagger \mathbf{C} \mathbf{w_U},$$

$$\mathbf{w_U}^\dagger \mathbf{H} \mathbf{w_U} \sim 0,$$

and their equivalents for downward-steered vectors.

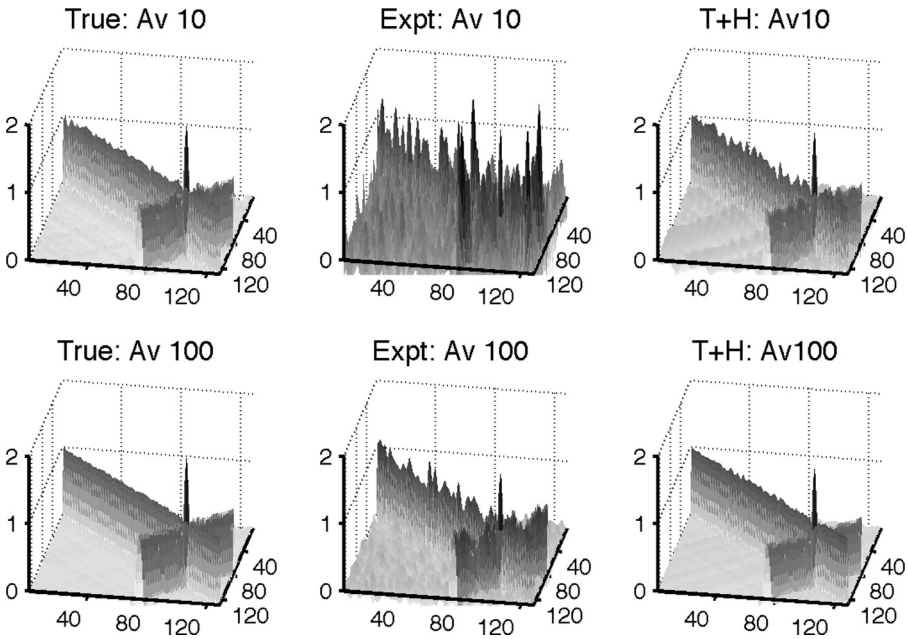

FIG. 1. Synthesised cross-spectral density matrix for a 128-element array at 1.5 kHz. Columns from left to right: True meaning each element is the integral over angle of the product of complex arrivals; Expt meaning each element is the integral over angle of the product of the already angle-integrated omnidirectional hydrophone signals; T+H meaning each element is the sum of the separated Toeplitz and Hankel parts. Top row is the average of 10 realisations; bottom row is the average of 100 realisations.

- For opposing steering vectors

$$\mathbf{w_D}^\dagger \mathbf{H} \mathbf{w_U} = \mathbf{w_D}^\dagger \mathbf{C} \mathbf{w_U},$$

$$\mathbf{w_D}^\dagger \mathbf{T} \mathbf{w_U} \sim 0.$$

(In all cases $\mathbf{C} = \mathbf{x}\,\mathbf{x}^\dagger$.)

At first sight, it is paradoxical that there is agreement between $\mathbf{w_U}^\dagger \mathbf{T} \mathbf{w_U}$ and $\mathbf{w_U}^\dagger \mathbf{C} \mathbf{w_U}$ and separately between $\mathbf{w_D}^\dagger \mathbf{H} \mathbf{w_U}$ and $\mathbf{w_D}^\dagger \mathbf{C} \mathbf{w_U}$, but in Fig. 1, on the other hand, there is much more fluctuation in $\mathbf{C}$ ($=\mathbf{x}\,\mathbf{x}^\dagger$) (labelled Expt) than in $\mathbf{T}+\mathbf{H}$ (labelled T+H). However the explanation is quite simple. Because $\mathbf{w_U}$, $\mathbf{w_D}$ are a conjugate pair $\mathbf{w_D}^\dagger \mathbf{C} \mathbf{w_U}$ could be written as $\mathbf{w_U}^{\mathbf{T}} \mathbf{C} \mathbf{w_U}$ (the T superscript signifying transpose without conjugate), so, as mentioned earlier, for arbitrary $\mathbf{R}$ the product $\mathbf{w_U}^{\mathbf{T}} \mathbf{R} \mathbf{w_U}$ is identical to the sum over all terms of the term-by-term product of $\mathbf{R}$ with the matrix $\mathbf{w_U}^{\mathbf{T}} \mathbf{w_U}$, which must be Hankel as long as the elements of $\mathbf{w_U}$ are of the form $\exp(i\,n\ldots)$. So, whether the matrix $\mathbf{R}$ is pre-summed along its anti-diagonals [as in Eq. (16) to form $\mathbf{H}$] or not, the term-by-term multiplication by the Hankel matrix $\mathbf{w_U}^{\mathbf{T}} \mathbf{w_U}$ will have the same effect as summing along the anti-diagonals. Thus, despite the noisy appearance of the Expt matrix $\mathbf{C}$ in Fig. 1, one still finds $\mathbf{w_U}^\dagger \mathbf{T} \mathbf{w_U} = \mathbf{w_U}^\dagger \mathbf{C} \mathbf{w_U}$ and $\mathbf{w_D}^\dagger \mathbf{H} \mathbf{w_U} = \mathbf{w_D}^\dagger \mathbf{C} \mathbf{w_U}$. This agreement is further borne out by the plots of impulse response using both derivations in Sec. IV.

IV. APPLICATION TO EXPERIMENTAL DATA

To compare performance of the separated Toeplitz and Hankel approach with the usual coherence matrix approach an experimental example is taken from some existing drifting 32-element vertical array data collected at approximately 15:45 on May 12, 2004 during the first drift over the Ragusa Ridge (see Harrison and Siderius, 2008, for experimental details). This data set was originally difficult to handle, and it was suspected by Harrison that this was due to the effect on integration time of wave induced oscillatory motion of the array in a heavy sea. Some simple order-of-magnitude calculations, knowing the mass of the ballast weight and the buoyancy per unit length of the flexible connecting cable, predicted an oscillation period of about 10 s. This period was subsequently confirmed as 7 s with amplitude 1 m (Traer and Gerstoft, 2011). The point of using the data in this paper is to demonstrate the success of this processing approach with a short integration time. To avoid blurring, processing needs to be completed in about $7/(2\pi)$ seconds, and in this time, with a sample rate of 12 kHz and 4096 samples per Fourier transform block, there are just over three blocks available.

The enlargement of the seabed impulse response in Fig. 2 is the result of averaging four blocks of 4096 samples. Travel time has been converted to two-way path length, and the y-axis labelled "Amplitude" is the absolute value of the Hilbert transform of the inverse Fourier transform of quantities in the text such as $\mathbf{w_D}^\dagger \mathbf{C} \mathbf{w_U}$. The three almost coincident lines correspond to processing with, respectively, the separated Hankel part alone ($\mathbf{w_D}^\dagger \mathbf{H} \mathbf{w_U}$), conventional ($\mathbf{w_D}^\dagger \mathbf{R} \mathbf{w_U}$) where $\mathbf{R} = \langle \mathbf{x}\mathbf{x}^\dagger \rangle$, and the sum of the separated Hankel and Toeplitz parts [$\mathbf{w_D}^\dagger (\mathbf{T}+\mathbf{H}) \mathbf{w_U}$].

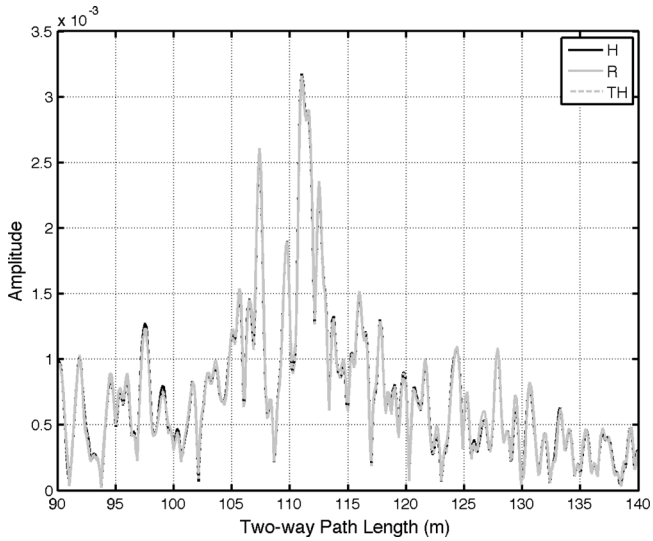

FIG. 2. Enlargement of the experimental impulse response resulting from the average of four blocks of 4096 samples calculated three ways: H uses the separated Hankel matrix; R uses the matrix constructed directly from the hydrophone inputs as $\mathbf{R} = \mathbf{x}\,\mathbf{x}^\dagger$; TH uses the sum of the separated Toeplitz and Hankel matrices. Differences are small through using Eqs. (13) and (16).

For comparison, and as an aide to identifying these three lines, Fig. 3 shows the same quantities but evaluating Eqs. (10) and (15) as numerical integrals discretized with 32 values of $\sin\theta$ strictly between 0 and 1, unlike the DFT. The earlier equations were in the frequency domain, for a single frequency. Comparing Figs. 2 and 3 the effects of discrepancies between the two approaches can be seen in the time domain.

Notice that the "H" and "TH" curves still agree very well, as one would expect because the Toeplitz part contributes essentially nothing. However, the "R" curve, that is unchanged from Fig. 2, has more peak-trough contrast than either H or TH curve, as one might expect from the smoothing effect of the convolution in Eq. (32).

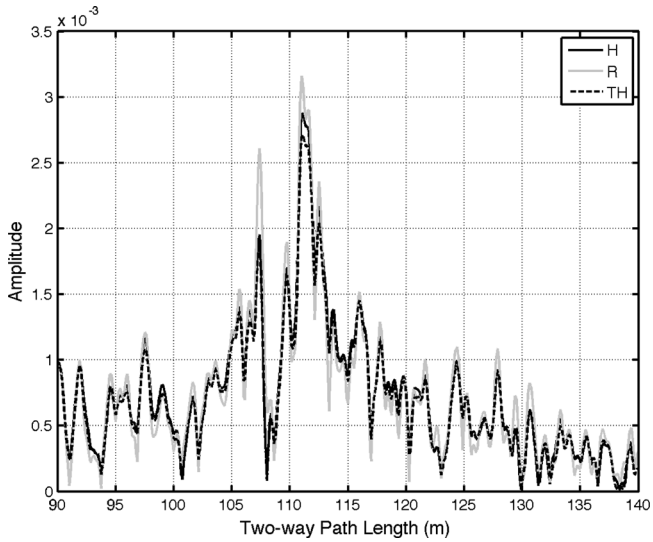

FIG. 3. Enlargement of the experimental impulse response as in Fig. 2 except that the Toeplitz and Hankel matrices were calculated with the different discretization of angle allowed by Eqs. (10) and (15). Differences are greater than in Fig. 2.

Disregarding the array motion Fig. 4 is the average of 200 Fourier transform blocks—there are roughly 20 Fourier transform blocks per full up-down cycle of the hydrophone array. Clearly, there are still two distinct peaks despite the broadening of a few metres and all three curves agree pretty well.

Otherwise the fact that there are still background fluctuations, particularly for path lengths less than about 108 m which correspond to locations above the seabed, indicates that the averaging of type 1 (in Sec. I) have not yet converged. Clearly, there is nothing to stop one increasing integration time indefinitely, but despite the similarity between Figs. 2 and 4 and the apparent smoothing benefit, small systematic shifts of the peaks in time would be smoothed out. This peak shifting is revealed by plotting the intensity of Fig. 2 against travel time (two-way path length) and hydrophone-array-drift time, i.e., a sub-bottom profile.

The sub-bottom profile, Fig. 5, obtained with a four-block average using the H processing corresponding to Fig. 2 shows the resolved periodic waves due to the array motion and the second reflection at a 3 m deeper round-trip path. At this geographic location, namely, the Ragusa Ridge, it is likely that there is a thin layer of sediment covering rock which explains the two arrivals.

It is interesting that, from an integration time point of view, there seem to be brighter spots (i.e., better convergence) at the location of the wave peaks and troughs rather than at the intervening slopes. One obvious reason is that on the slopes the amplitude contributions are shared out between different time bins. A more subtle reason is that the motion causes a mismatch between the up- and down-beam time series, i.e., a very small, but possibly significant, Doppler shift. It can be seen that these two mechanisms, though related, are distinct by thinking of the first as the array passing through many depths but being stationary at each one; this leads to weakening through blurring but without Doppler effect. In contrast the second mechanism must include Doppler.

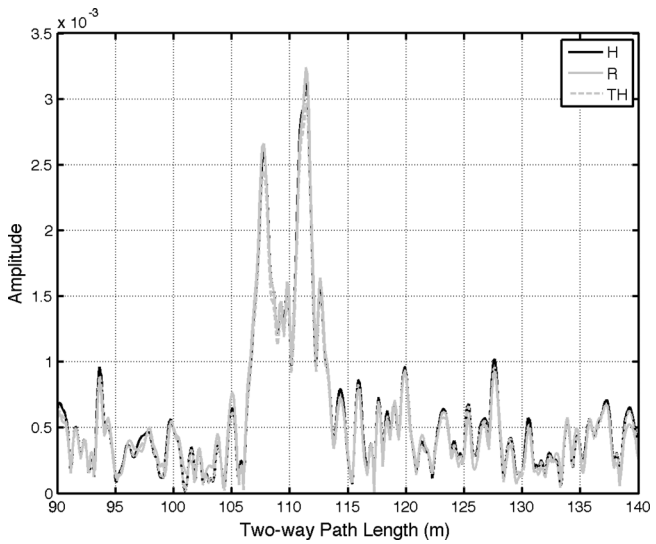

FIG. 4. The same enlargement of the experimental impulse response as in Figs. 2 and 3 but averaging over 200 blocks (roughly nine cycles of array oscillation) and disregarding the array's motion.

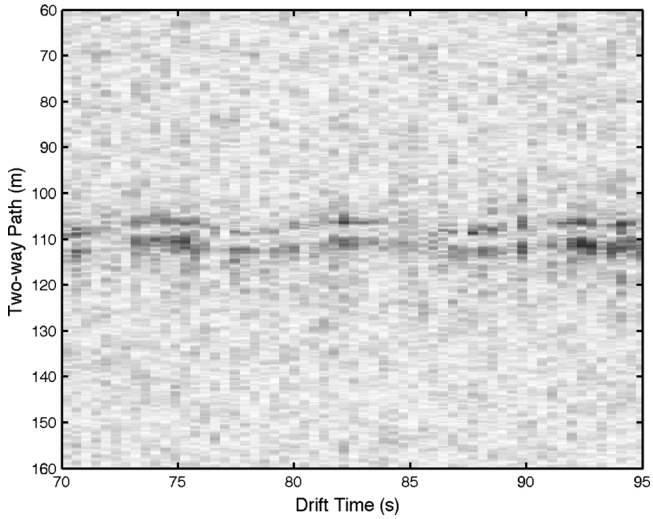

FIG. 5. Enlargement of a sub-bottom profile showing two layer boundaries contaminated by array oscillations of about 1 m and period roughly 7 s.

V. CONCLUSIONS

This paper set out to search for an alternative computational route to the function $\mathbf{w_D}^\dagger \mathbf{C} \mathbf{w_U}$, which is an essential component in the calculation of the seabed's impulse response, or time domain Green's function, the hope being that convergence might be more rapid. It was noted that the infinitely averaged coherence of sea surface noise naturally separates into Toeplitz and Hankel parts [Eq. (5)]. A practical basis for this separation with experimental data was proposed [Eqs. (9), (10), and (15)], and the derivation extended to show that $\mathbf{w_D}^\dagger \mathbf{C} \mathbf{w_U} = \mathbf{w_D}^\dagger (\mathbf{T}+\mathbf{H}) \mathbf{w_U}$ could be reduced to $(\mathbf{w_D x}^\dagger)(\mathbf{w_U x}^\dagger)^\dagger$ [Eq. (34)]. Since the latter is already identically equal to $\mathbf{w_D}^\dagger \mathbf{C} \mathbf{w_U}$, not only is the proof tied down at both ends, but furthermore whichever of the four ways the calculation is done [i.e., Hankel alone, Hankel plus Toeplitz, the product $(\mathbf{w_D x}^\dagger)(\mathbf{w_U x}^\dagger)^\dagger$, or the ordinary coherence matrix $\mathbf{w_D}^\dagger \mathbf{R} \mathbf{w_U}$ using $\mathbf{R} = \langle \mathbf{x x}^\dagger \rangle$] the result is the same to within numerical accuracy. Therefore none of these approaches has any particular advantage from the point of view of improving convergence and reducing the integration time. However, there is a clear winner from the point of view of processing time and that is the product $(\mathbf{w_D x}^\dagger)\ (\mathbf{w_U x}^\dagger)^\dagger$, which requires $2N_h+1$ multiplications as opposed to the $2N_h{}^2$ multiplications for $\mathbf{w_D}^\dagger \mathbf{R} \mathbf{w_U}$. The Toeplitz and Hankel calculations each require an additional pair of Fourier transforms.

It was found that the Toeplitz matrix can be seen as either the spatial auto-correlation of the hydrophone responses, or the sums down the offset diagonals of the matrix $\mathbf{x x}^\dagger$ [Eq. (13)]. Similarly the Hankel matrix can be seen as either the spatial cross-correlation of the hydrophone responses with the same responses in reverse order (i.e., the convolution of the response with itself), or the sums down the offset anti-diagonals of the matrix $\mathbf{x x}^\dagger$ [Eq. (16)]. A rather surprising result is that even if the hydrophones are not uniformly spaced the coherence can still be separated into a Toeplitz and Hankel part.

A simple simulation of directional noise (Fig. 1) demonstrated the behaviour of three calculations of CSDM after light or intensive averaging. The "Toeplitz + Hankel" matrix [Eqs. (9), (10), and (15) or (13) and (16)] is much less chaotic than the $\mathbf{x}\,\mathbf{x}^{\dagger}$ matrix used in the standard processing case [Eq. (1)] and approaches the perfection of the "true" coherence. A summary was given of the properties of the various scalar products of CSDMs with up- or down-steering vectors. It was explained that despite the reduced fluctuation in the Toeplitz and Hankel matrix, as compared with the $\mathbf{x}\,\mathbf{x}^{\dagger}$ matrix, the fact that the steering vector $\mathbf{w_U}$ is of the form $\exp(i\ n\ldots)$ and $\mathbf{w_D}$ is its conjugate means that a product such as $\mathbf{w_D}^{\dagger}\mathbf{C}\mathbf{w_U}$ is equal to $\mathbf{w_D}^{\dagger}\mathbf{H}\mathbf{w_U}$ since the matrix multiplication operation effectively already sums along the anti-diagonals.

The Toeplitz and Hankel separation was applied to some experimental drifting vertical array data in a sub-bottom profiling application. The deliberately chosen data suffered from wave induced oscillation of the array making integration time a serious issue (Figs. 4 and 5). A comparison of the impulse response calculated using the separated Hankel matrix and using the original coherence matrix showed that agreement was extremely good when using the DFT form [Eq. (13) and (16); Fig. 2] and slightly less good when using an arbitrary number of points to discretize $\sin\theta$ in the Fourier transform (Fig. 3).

Finally, it was noted that, as might be expected, convergence was better at the peaks and troughs of the array's motion. The poorer convergence in between clearly needs more time whether allowance for Doppler is required or not.

ACKNOWLEDGMENTS

The author thanks Peter Nielsen for many stimulating discussions on this subject. He also thanks the Captain and crew of the *NRV Alliance* and CMRE engineering staff for facilitating collection of noise data during the experiments, and more recently CMRE for supplying an Emeritus office and other facilities after his retirement.

[1]Note that the factor $2\pi/(Nkd)$ can be written in terms of the design frequency f_o as $2f_o/(fN)$ so that for frequencies below the design frequency samples of a exist with value zero but outside the real range of θ.

[2]In proprietary software an auto-correlation as in Eq. (13) would in any case be computed via DFTs, thus the result would naturally be a cyclic auto-correlation. In contrast, an "unbiased" cross-correlation compensates for the shorter lengths of the outer diagonals. We shall return to this point in more detail in Sec. II C.

Gerstoft, P., Hodgkiss, W. S., Siderius, M., Huang, C. F., and Harrison, C. H. (**2008**). "Passive fathometer processing," J. Acoust. Soc. Am. **123**, 1297–1305.

Harrison, C. H. (**1996**). "Formulas for ambient noise level and coherence," J. Acoust. Soc. Am. **99**, 2055–2066.

Harrison, C. H. (**2004**). "Sub-bottom profiling using ocean ambient noise," J. Acoust. Soc. Am. **115**, 1505–1515.

Harrison, C. H. (**2005**). "Performance and limitations of spectral factorization for ambient noise sub-bottom profiling," J. Acoust. Soc. Am. **118**, 2913–2923.

Harrison, C. H. (**2009**). "Anomalous signed passive fathometer impulse response when using adaptive beam forming (L)," J. Acoust. Soc. Am. **125**, 3511–3513.

Harrison, C. H., and Siderius, M. (**2008**). "Bottom profiling by correlating beam-steered noise sequences," J. Acoust. Soc. Am. **123**, 1282–1296.

Harrison, C. H., and Simons, D. G. (**2002**). "Geoacoustic inversion of ambient noise: A simple method," J. Acoust. Soc. Am. **112**, 1377–1389.

Muzi, L., Siderius, M., Quijano, J. E., and Dosso, S. E. (**2015**). "High-resolution bottom-loss estimation using the ambient-noise vertical coherence function," J. Acoust. Soc. Am. **137**, 481–491.

Quijano, J. E., Dosso, S. E., Dettmer, J., Zurk, L. M., Siderius, M., and Harrison, C. H. (**2012**). "Bayesian geoacoustic inversion using wind-driven ambient noise," J. Acoust. Soc. Am. **131**, 2658–2667.

Siderius, M., Harrison, C. H., and Porter, M. B. (**2006**). "A passive fathometer technique for imaging seabed layering using ambient noise," J. Acoust. Soc. Am. **120**, 1315–1323.

Siderius, M., Song, H., Gerstoft, P., Hodgkiss, W. S., Hursky, P., and Harrison, C. (**2010**). "Adaptive passive fathometer processing," J. Acoust. Soc. Am. **127**, 2193–2200.

Traer, J., and Gerstoft, P. (**2011**). "Coherent averaging of the passive fathometer response using short correlation time," J. Acoust. Soc. Am. **130**, 3633–3641.

Young, V. (**2005**). "Using a vertical line array and ambient noise to obtain measurements of seafloor reflection loss," Report SR-410, NATO Undersea Research Centre, La Spezia, Italy.

Document Data Sheet

Security Classification		Project No.
Document Serial No.	**Date of Issue**	**Total Pages**
CMRE-PR-2017-001	August 2017	9 pp.

Author(s)

Harrison, C.H.

Title

Separation of measured noise coherence matrix into Toeplitz and Hankel parts.

Abstract

The cross-spectral density of ocean ambient noise is usually estimated from the product of the com-plex hydrophone signals, each of which already corresponds to the summed responses of sources from all angles. The true coherence is the integral over all angles of the angle-dependent product. The influence of this distinction on necessary time integration in geoacoustic inversion and passive fathometry is explored, and a meaningful separation of the cross-spectral density matrix into Toeplitz and Hankel parts is proposed. Various processing techniques are applied to synthesized data and some experimental vertical array data in a passive fathometry context. Passive fathometry is only sensitive to the Hankel part of the matrix.

Keywords

Issuing Organization

Science and Technology Organization
Centre for Maritime Research and Experimentation

Viale San Bartolomeo 400, 19126 La Spezia, Italy

[From N. America:
STO CMRE
Unit 31318, Box 19, APO AE 09613-1318]

Tel: +39 0187 527 361
Fax:+39 0187 527 700

E-mail: library@cmre.nato.int